High conductive Ag nanowire–polyimide composites: Charge transport mechanism in thermoplastic thermostable materials

Thanh Hoai Lucie Nguyen, Luis Quiroga Cortes, Antoine Lonjon, Eric Dantras, Colette Lacabanne

High conductive Ag nanowire–polyimide composites: Charge transport mechanism in thermoplastic thermostable materials

Thanh Hoai Lucie Nguyen, Luis Quiroga Cortes, Antoine Lonjon, Eric Dantras *, Colette Lacabanne

Physique des Polymères, CIRIMAT/Institut Carnot, Université Paul Sabatier, 118 route de Narbonne, 31062 Toulouse Cedex 9, France

A B S T R A C T

High conductive composites were elaborated by incorporating high aspect ratio (250) silver nanowires in polyimide matrix via solvent mixing way. Silver nanowires were synthesized in solution by polyol synthesis. The composite conductivity reaches the value of 10^2 $S \cdot m^{-1}$ above a very low percolation threshold (0.48 vol.% of silver nanowires). SEM-FEG images showed that metallic nanowires are well dispersed in PI matrix. They do not influence the physical structure of the polymer. Below the percolation threshold, γ, β and α relaxation modes were detected. γ relaxation mode was fitted to determinate the activation energy value (32.7 $kJ \cdot mol^{-1}$) and the relaxation time (1.5×10^{-16} s). The mobility associated with the γ relaxation is considered to be localized and non-cooperative. According to the Mott theory, studies on composites below the percolation threshold showed that the conduction mechanism is ruled by tunneling at low temperatures. The transport mechanism led by hopping is activated at −50 °C.

1. Introduction

High aspect ratio particles have a great interest in conductive polymer matrix composite elaboration. They allow getting high performance composites at a very low content. A low concentration of fillers, homogeneously dispersed, enables to maintain the mechanical performance of polymer matrix and its processability. Polymers have been filled with different high aspect ratio particles (carbon nanotubes [1] and metallic wires [2]) to obtain conductive materials with a low percolation threshold. As far as we know, metallic wires are the best candidates to elaborate a composite with the highest conductivity above percolation threshold [3]. Polyimides present good chemical resistance, high thermal stability, and high mechanical strength. They are widely applied in aerospace as high performance engineering materials and in microelectronic industry as flexible substrates and dielectric layers [4–6]. For these applications it is desirable to use polyimides that are soluble in coating and casting processes [7]. The good dielectric properties of polyimides induce static charge accumulation problem. Their dissipation with preservation of mechanical properties is a great challenge. In order to increase the electrical conductivity, carbon black and carbon nanotubes have been already introduced in polyimides [4,5]. For polyimide/carbon nanotube composites, the electrical conductivity reached 10^{-5} $S \cdot m^{-1}$ for 3 wt.% [4] and 10^{-4} $S \cdot m^{-1}$ for 8 vol.% [8]. Carponcin et al. [9] obtained 10^{-1} $S \cdot m^{-1}$ in polyamide 11 for a loading of 0.96 wt.%. It was shown that elaboration of high electrical conductive polyimide is difficult. The highest values of conductivity reported in literature are for polymers filled with metallic particles [10]. The conductivity of a polymer matrix filled with metallic particles can be limited by the surface oxidation [3]. Ag nanowires are good candidates because they are preserved from surface oxidation layer. Recent studies showed that P(VDF-TrFE) matrix filled with Ag nanowires reaches 10^2 $S \cdot m^{-1}$ for a very low percolation threshold (0.63 vol.%) [11].

Ag NWs have been synthetized by the reduction of $AgNO_3$ in ethylene glycol solutions containing poly(vinyl pyrrolidone) (PVP) [12–14]. Literature reports several other methods: synthesis in aqueous solutions in the presence or absence of seeds and surfactants [15–18], hydrothermal synthesis using glucose as reducing agent [19], microwave assisted synthesis [20], and using template-directed synthesis in AAO [3]. But these elaboration techniques do not allow obtaining large quantities. In this work, Ag nanowires will be prepared by polyol process. They will be introduced in a polyimide matrix in order to reach a high electrical conductivity at a very low percolation threshold. Physical structure and electrical behavior of the matrix and of the composites will be studied.

2. Materials and methods

2.1. Materials

Polyimide (PI)/1-ethyl-2-pyrrolidone (NEP) solution (25 wt.%) was supplied by Evonik, Germany. Electroless Ag nanowires (Ag NWs) were synthesized by reducing $AgNO_3$ with ethylene glycol in the presence of poly(vinyl pyrrolidone). The reaction was carried out at 160 °C in a round-bottom balloon with magnetic stirring bar. This method and the solution concentrations were described by Sun et al. [13,14]. This method allows obtaining Ag NWs with a length distribution

* Corresponding author.
E-mail address: eric.dantras@univ-tlse3.fr (E. Dantras).

between 30 and 60 μm and a diameter around 200 to 300 nm. The Ag NWs morphology was characterized by SEM-FEG to estimate the mean aspect ratio ξ. The Ag NW suspension was rinsed in water and filtered through a polyamide (200 nm pore size) membrane. Filtered Ag NWs were stored in NEP and dispersed using a short pulse of sonication during 5 s, corresponding to a 25 W dissipated power.

2.2. Polyimide/Ag NW composite elaboration

A volume of Ag NW suspension was added to the PI/NEP solution under sonification. This suspension was film coated on a glass plate and placed in an oven at 80 °C during 30 min to evaporate the solvent. The film was removed from the glass plate and heated at 300 °C during 2 h in order to evaporate the residual traces of NEP. The formed composite was a film with a thickness around 50 μm. PI/Ag NW composites were elaborated with a volume fraction varying from 0 to 3 vol.%.

2.3. Scanning electron microscopy

The morphology of Ag NWs was observed by scanning electron microscopy (SEM) using a JEOL JSM 6700F instrument equipped with a field emission gun (SEM-FEG). The composites were fractured at the liquid nitrogen temperature to be observed by SEM-FEG.

2.4. Differential scanning calorimetry

Composite glass transition phenomenon was investigated by differential scanning calorimetry (DSC) using a TA Instrument 2920 DSC. Thermogravimetric analysis does not show degradation until 500 °C. DSC experiments were carried out in the temperature range 200–380 °C with a constant heating rate of 20 °C·min^{-1}. All the DSC measurements were performed under helium atmosphere. The DSC thermograms, reported in Fig. 3, represent the evolution of the heat capacity for neat PI and its composites filled with 0.5, 1, 1.5, 2, 2.5 and 3 vol.% of Ag NWs (Table 1).

2.5. Broadband dielectric spectrocopy

A BDS 4000 Novocontrol broadband dielectric spectrometer (BDS) system was used to obtain the dielectric relaxation map in a wide temperature and frequency range. The sample was inserted between two plan parallel electrodes. It was stimulated by a sinusoidal electrical field for an isothermal temperature and the complex impedance is recorded during frequency scan. The measurements were carried out in the frequency range 10^{-1}–10^{6} Hz from −150 to 250 °C by steps of 5 °C. This technique has been extensively described by Kremer and Schonhals [21]. In order to distinguish the influence of heating on the samples, two cycles of dielectric measurements were performed in this temperature range. The complex dielectric permittivity $\varepsilon^*_T(\omega)$ was recorded.

Relaxation modes were fitted with the Havriliak–Negami equation [22]:

$$\varepsilon^*_{T(\omega)} = \varepsilon_\infty + \frac{\varepsilon_S - \varepsilon_\infty}{(1 + (i\omega\tau_{HN})\alpha_{HN})\beta_{HN}} \quad (1)$$

where ε_∞ is the relative real permittivity at infinite frequency, ε_S is the relative real permittivity at zero frequency, τ_{HN} is the relaxation time, α_{HN} and β_{HN} are the Havriliak–Negami parameters and ω is the angular frequency.

Dipolar relaxations are often hidden by dissipative losses due to ohmic conduction. The Kramers–Kronig transform [23] offers an analytical tool to calculate ε''_{KK} from the real part $\varepsilon'_T(\omega)$:

$$\varepsilon''_{KK(\omega_0)} = \frac{\sigma_0}{\varepsilon_0\omega_0} + \frac{2}{\pi}\int_0^\infty \varepsilon'_{(\omega)} \frac{\omega_0}{\omega^2 + \omega_0^2} \cdot d\omega. \quad (2)$$

2.6. Electrical conductivity

The electrical conductivity of the PI/Ag NW composites was measured by a four wire sensing method using a Keithley 2420 when the sample resistance measured was below 100 Ω. When the value was above 100 Ω, electrical conductivity measurements were carried out by recording the complex conductivity $\sigma^*(\omega)$ using a Novocontrol broadband spectrometer. Measurements were done in the frequency range from 10^{-2} to 10^{6} Hz at room temperature. The real part, $\sigma'(\omega)$ of the complex conductivity $\sigma^*(\omega)$ was investigated. The value of $\sigma'(\omega)$ at 10^{-2} Hz was taken as dc conductivity σ_{dc} [1]. 50 μm thick film composites were placed between two circular gold platted electrodes (20 mm in diameter). To reduce contact resistivity with the cell electrodes, a thin silver lacquer layer was coated onto both sides of the films.

3. Results and discussion

3.1. Microscopic observation

The morphology and aspect ratio of Ag NWs were studied by SEM-FEG with secondary electron detection mode. Dispersed Ag NWs in NEP suspension are deposited on SEM pin. After NEP evaporation, Ag NWs are shown in Fig. 1. Individually nanowires are observed. They have no affinity with NEP, which allows a homogeneous dispersion in this solvent. They were not damaged after sonication treatment. Ag NW widths were ranged from 200 to 300 nm, and their lengths from 20 to 80 μm. However, we estimated that at least 70% of the nanowires were over 60 μm long which meant low size dispersion. The mean aspect ratio of silver nanowires was estimated around 250. Sun et al. [14] measured an intrinsic conductivity of 0.8×10^7 S·m^{-1} for a single Ag NW. Ag NWs observed indicate the interest of this method to obtain reproducible and large quantity of Ag NWs. PI/Ag NW composites were prepared with Ag NW volume fractions from 0.25 vol.% to 3 vol.%. Fig. 2 shows SEM-FEG cryocuts of the PI matrix filled with 0.5 and 3 vol.%. Films were fractured at liquid nitrogen temperature perpendicularly to the stretching direction. Bright domains show that the Ag NWs dispersed in the PI matrix. Ag NWs were uniformly distributed throughout the PI matrix and micron size aggregates were not observed. Indeed, NWs have no affinity in NEP and they kept their homogeneous dispersion in the polymer.

3.2. Physical structure

DSC thermograms of neat PI and its composites filled with 0.5, 1, 1.5, 2, 2.5 and 3 vol.% of Ag NWs are reported in Fig. 3. The second temperature scans are shown. Because of its amorphous nature, PI glass transition is studied. For the neat PI, the T_g is near 330 °C. The glass transition temperature exhibits a very slight modification with the filler content.

Table 1
Glass transition temperatures and heat capacity step at T_g of PI/Ag composites.

Volume fraction of Ag NWs (vol.%)	0	0.5	1.0	1.5	2.0	2.5	3
T_g (°C)	329 ± 2	331 ± 2	326 ± 2	327 ± 2	327 ± 2	327 ± 2	327 ± 2
ΔC_p (J·g^{-1}.°C^{-1})	0.30 ± 0.01	0.27 ± 0.01	0.26 ± 0.01	0.23 ± 0.01	0.20 ± 0.01	0.31 ± 0.01	0.21 ± 0.01

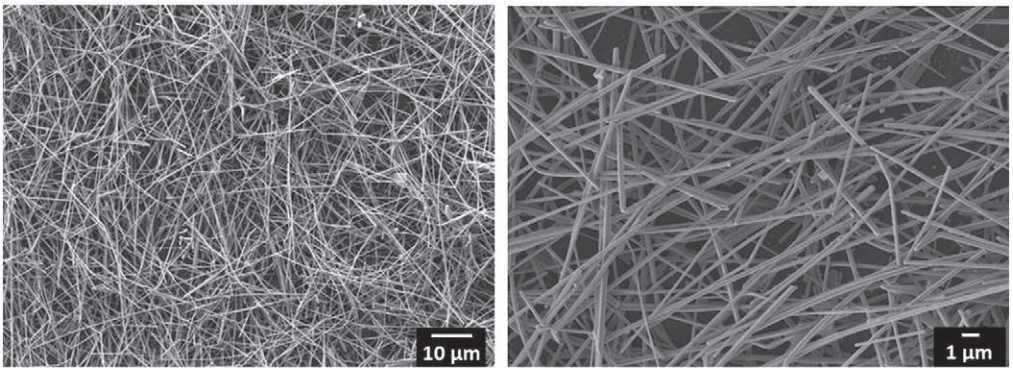

Fig. 1. SEM-FEG images of Ag NWs.

This variation is not significant. We consider that the addition of Ag NWs does not have impact on PI physical structure (Table 1).

3.3. Dielectric behavior of PI matrix

BDS measurements allowed us to observe the dielectric loss ε″ versus frequency and temperature. Two consecutive temperature scans were carried out. In the low temperature range, a γ relaxation is pointed out. For the second scan, relaxation strength of this local mode decreases, as it is showed in Fig. 4. In the literature, most of the authors associated γ relaxation with the mobility of the complex solvent/polar groups [24]. Solvent molecules interact with polar groups of the polyimide chain. This is confirmed by the mode decrease on the second scan which highlights the NEP molecule removal during the first scan. γ relaxation is related with NEP traces in the sample. Fig. 5 represents the evolution of relaxation time τ_{HN} on the Arrhenius diagram. The relaxation time was fitted with the Arrhenius equation:

$$\tau(T) = \tau_0 \exp\frac{E_a}{RT} \tag{3}$$

where τ (T) is the relaxation time, E_a is the apparent activation energy of the process, R is the gas constant, τ_0 is the pre-exponential factor. For γ relaxation and between the first and the second temperature scans, τ_0 values decrease from 2.0×10^{-15} s to 1.5×10^{-16} s. E_a values decrease from 46.5 kJ·mol^{-1} to 32.7 kJ·mol^{-1}. Relaxation time behavior and $\Delta\varepsilon_\gamma$ evolution are associated with NEP trace desorption in the sample. This polar molecule is removed from the PI film during the first scan. Activation parameter value for the second scan is coherent with previous studies with polyimide [24–26]. E_a and τ_0 provide information on domain size where cooperative mobility takes place and the mobility nature involved in the relaxation process. E_a value is low and τ_0 is relatively close to the Debye time ($\tau_D = 10^{13}$ s = 2πh / kT at room temperature), the mobility associated with the γ relaxation in polymer is considered localized and non-cooperative [27].

At high temperature and low frequency, the imaginary part of the dielectric permittivity increases due to the contribution of charge carriers' mobility. In order to observe higher temperature relaxations hidden by dissipative losses due to conduction, ε''_{KK} is calculated from $\varepsilon'_{T(\omega)}$ of the second temperature scan. Dielectric permittivity ε''_{KK} is represented as a function of frequency and temperature in Fig. 6. In spite of this analytical tool, relaxation time extraction of β and α modes remains difficult.

3.4. Electrical conductivity

3.4.1. Percolation threshold

The composite electrical conductivity is reported as the function of the Ag NW volume fraction in Fig. 7. The pure PI electrical conductivity is measured near 10^{-14} S·m^{-1}. The conductivity increased drastically from 10^{-14} to 10^{2} S·m^{-1}. The conductivity has been measured on two samples for each rate of Ag NWs and the standard deviation has been calculated with these two values. In three-dimensional disordered systems, the insulator to conductor transition is marked by the percolation threshold. The sixteen decade gap between insulator–conductor behaviors highlights the electrical percolation phenomenon. The following scaling equation, proposed by Kirkpatrick [28], links the evolution of the conductivity to four parameters:

$$\sigma_{DC} = \sigma_0(p - p_C)^t \tag{4}$$

where σ_0 is a constant, p the volume fraction of Ag NWs, p_C the Ag NW volume fraction at the percolation threshold, and t the critical exponent. The best fitted values are obtained for $p_C = 0.48$ vol.%, $\sigma_0 = 1.44 \times 10^7$ S·m^{-1} and $t = 3.4 \pm 0.5$. The very low percolation threshold confirms the high aspect ratio of Ag NWs. The percolation threshold is one of the lowest observed in literature for such particles [11,29,30] in thermoplastic polymer matrix.

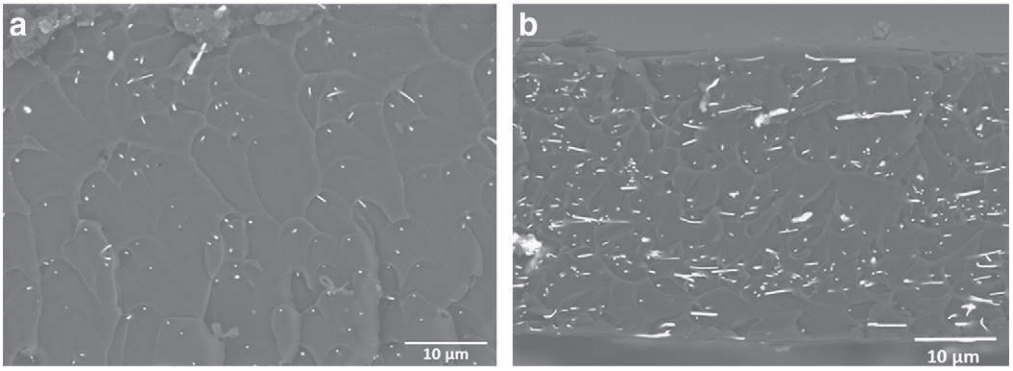

Fig. 2. SEM-FEG images of cryo fractures of composites PI/Ag NWs: (a) 0.5 vol.%, (b) 3 vol.%.

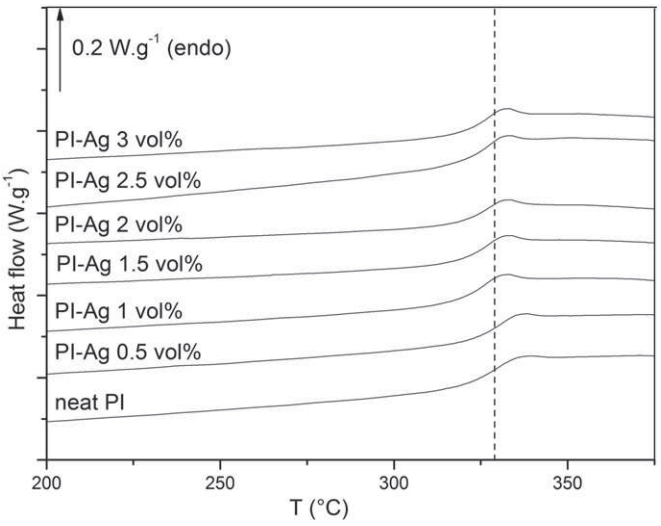

Fig. 3. DSC thermograms of neat PI and its composites filled with 0.5, 1, 1.5, 2.5 and 3 vol.% of Ag NWs.

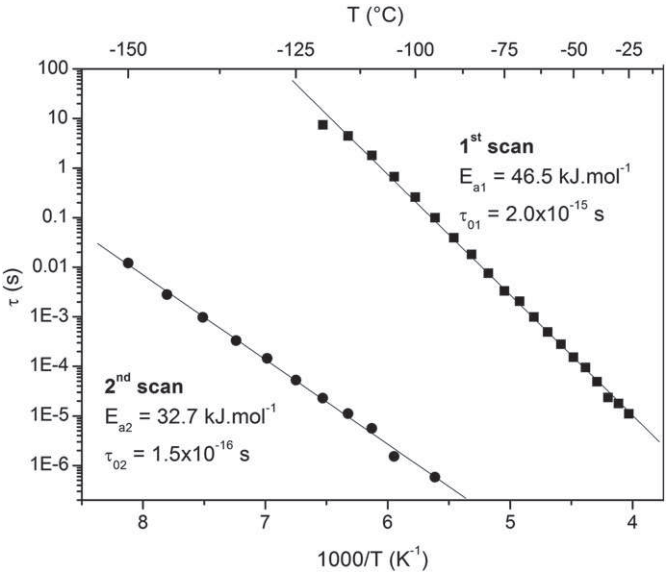

Fig. 5. Dependence of τ_{HN} on temperature for neat PI at the 1st and the 2nd measurements.

The t exponent is slightly higher than the universal value predicted the percolation theory by Stauffer [31] associated with a 3D percolation network which is between 1.6 and 2. Such gaps have been observed before [3,9]. However, the value of t is in the same order of magnitude than the universal value which shows that the percolation occurs in a 3D network.

The conductivity above percolation threshold is similar to the values of 10^2 $S \cdot m^{-1}$ reported in the literature [10,11] for various polymer matrices. This result demonstrates that this value is not dependent from the physical structure and/or the dielectric permittivity of the matrix.

3.4.2. Temperature dependence of DC conductivity below percolation threshold

This composite is considered as a homogeneous system because Ag NWs are uniformly dispersed in PI matrix. Above the percolation threshold, the level of electrical conductivity is not adapted for dynamic conductivity measurement. Therefore, measurements are made with composite filled before and close to the percolation threshold. In order to study the charge transport mechanism and to confirm the Mott theory [32], the electrical DC conductivity of composites filled with 0.25 vol.% of Ag NWS is reported as the function of $100/T^{1/4}$ on Fig. 8.

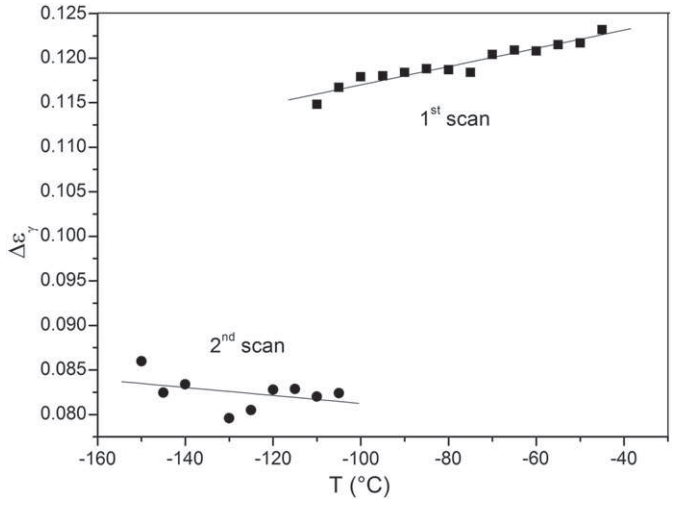

Fig. 4. Dielectric relaxation strength as a function of the temperature.

In homogeneous systems, the Mott theory describes the electronic state localization case around Fermi level with an exponential decay of charge carrier wave function. Charge transport takes place between these localized states. Charge carriers hop from a localized state to a nearby localized state of different or similar energy with special separation from the initial site. This mechanism is Variable Range Hopping (VHR) between localized states around Fermi level. The following equation describes the dependence of electrical conductivity with temperature:

$$\sigma = \sigma_0 e^{\left(\frac{T_0}{T}\right)^{\gamma}}. \quad (5)$$

σ_0 is a constant, $\gamma = \frac{1}{1+d}$ is dependent on system dimension d (1, 2 or 3), and T_0 is the Mott characteristic temperature. T_0 is dependent on localization length and on their density at Fermi level.

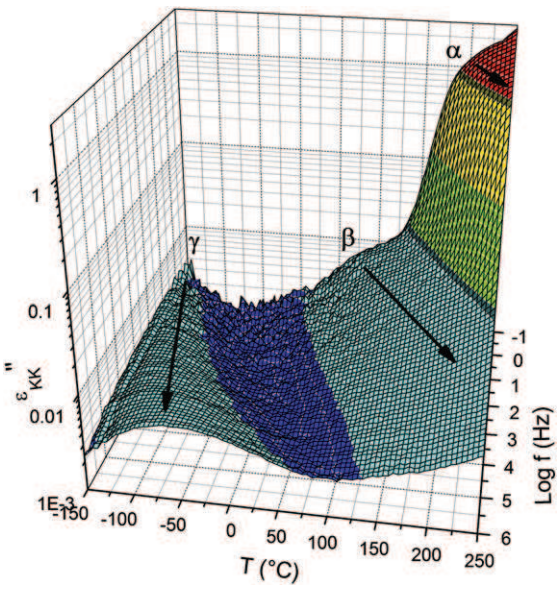

Fig. 6. ε''_{KK} deduced from $\varepsilon'_{T(\omega)}$ by analytical Kramers–Kronig transform.

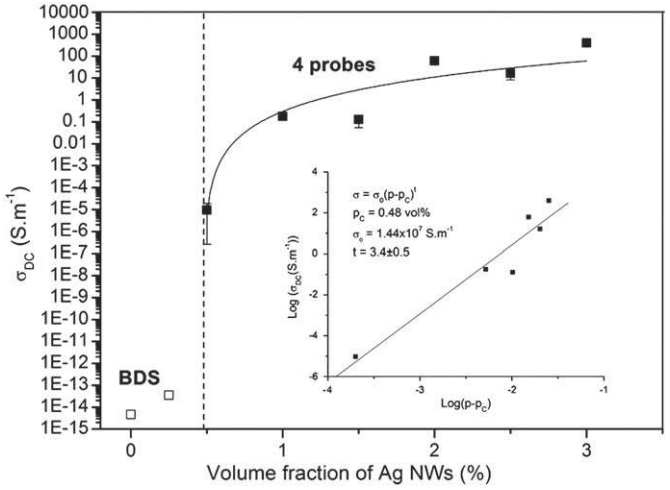

Fig. 7. Dependence of the DC conductivity on the Ag NW volume fraction in polyimide matrix at 25 °C, (□) measurement by BDS, (■) measurement by 4 wires.

To highlight dipolar relaxation influence on σ_{DC}, neat PI ε''_{KK} is also represented as a function of $100/T^{1/4}$ on this figure. DC conductivity behavior with temperature is influenced by neat PI dielectric behavior. Below −100 °C, the influence of γ relaxation mode on conductivity is observed. Above 25 °C, β and α modes also interfere on conductivity. Between these two temperature ranges there is no dipolar relaxation. It is possible to determinate the conduction mechanism. Below −50 °C, DC conductivity is independent on temperature which is typical of tunneling where the charge carrier crosses a potential barrier between two localized states. Above −50 °C, DC conductivity evolves linearly with $1/T^{1/4}$; the transport mechanism is activated by temperature. According to Mott, the conduction behavior is led by hopping.

4. Conclusion

PI–Ag NW composite elaboration and their electrical properties are described. At the microscopic level, the Ag nanowires were quasi-randomly distributed in the PI matrix. The PI glass transition near 330 °C was determined by DSC. This value is independent from Ag NW fraction in the composite. The percolation threshold was one of the lowest observed in the literature (p_C = 0.49 vol.%) for thermoplastic matrix. The addition of Ag NWs into the PI matrix increased the conductivity by 16 orders of magnitude and reached a conductivity value of 10^2 S·m^{-1}. This conductivity level above the percolation threshold is coherent with previous work of the group. The dielectric properties of PI matrix have been investigated. Three relaxations have been observed. Only γ relaxation corresponding to localized and non-cooperative mobility has been followed. The Arrhenius relaxation time behavior of this mode is strongly dependent from polar solvent molecule trace which has been totally removed for the second scan. These dipolar relaxations influence the DC conductivity mechanism. Nevertheless tunneling and hopping mechanism have been observed in this composite for various temperature ranges below the percolation threshold.

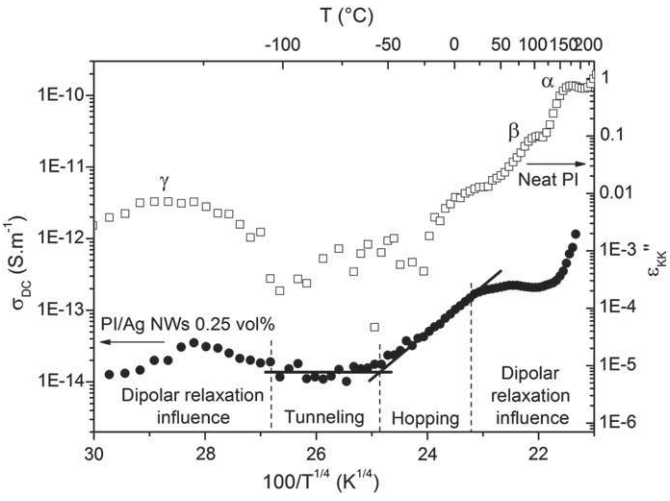

Fig. 8. Dependence of DC conductivity (•) on temperature for PI filled with 0.25 vol.% of Ag NWs and dependence of ε''_{KK} (□) on temperature for neat PI.

References

[1] S. Barrau, P. Demont, E. Perez, A. Peigney, C. Laurent, C. Lacabanne, Effect of palmitic acid on the electrical conductivity of carbon nanotubes–epoxy resin composites, Macromolecules 36 (2003) 9678–9680.
[2] S. Bhattacharrya, S.K. Saha, D. Chakravorty, Nanowire formation in a polymeric film, Appl. Phys. Lett. 76 (26) (2000) 3896.
[3] A. Lonjon, L. Laffont, P. Demont, E. Dantras, C. Lacabanne, New highly conductive nickel nanowire-filled P(VDF-TrFE) copolymer nanocomposites — elaboration and structural study, J. Phys. Chem. 113 (2009) 12002–12006.
[4] Q.-Y. Tang, Y.-C. Chan, N.-B. Wong, R. Cheung, Surfactant-assisted processing of polyimide/multiwall carbon nanotube nanocomposites for microelectronics applications, Polym. Int. 59 (9) (2010) 1240–1245.
[5] I.H. Tseng, H.C. Lin, M.H. Tsai, D.S. Chen, Thermal conductivity and morphology of silver-filled multiwalled carbon nanotubes/polyimide nanocomposite films, J. Appl. Polym. Sci. 126 (2012) E182–E187.
[6] C. Kizilkaya, F. Dumludag, S. Karatas, N.K. Apohan, A. Altindal, A. Gungor, The effect of titania content on the physical properties of polyimide/titania nanohybrid films, J. Appl. Polym. Sci. 125 (5) (2012) 3802–3810.
[7] Q. Zhang, G. Chen, S. Zhang, Synthesis and properties of novel soluble polyimides having a spirobisindane-linked dianhydride unit, Polymer 48 (8) (2007) 2250–2256.
[8] P. Murugaraj, D.E. Mainwaring, N. Mora-Huertas, Electromechanical response of semiconducting carbon-polyimide nanocomposite thin films, Compos. Sci. Technol. 69 (14) (2009) 2454–2459.
[9] D. Carponcin, E. Dantras, G. Aridon, F. Levallois, L. Cadiergues, C. Lacabanne, Evolution of dispersion of carbon nanotubes in polyamide 11 matrix composites as determined by DC conductivity, Compos. Sci. Technol. 72 (4) (2012) 515–520.
[10] M.P. Alvarez, V.H. Poblete, M.E. Pilleux, V.M. Fuenzalida, Submicron copper-low-density polyethylene conducting composites: structural, electrical, and percolation threshold, J. Appl. Polym. Sci. 99 (6) (2006) 3005–3008.
[11] A. Lonjon, P. Demont, E. Dantras, C. Lacabanne, Low filled conductive P(VDF-TrFE) composites: influence of silver particles aspect ratio on percolation threshold from spheres to nanowires, J. Non-Cryst. Solids 358 (23) (2012) 3074–3078.
[12] J.M. Zhang, D.Y. Shen, Evidence for the monolayer assembly of poly(vinylpyrrolidone) on the surfaces of silver nanowires, J. Phys. Chem. 108 (2004) 12877–12881.
[13] Y. Sun, B. Mayers, T. Herricks, Y. Xia, Polyol synthesis of uniform silver nanowires — a plausible growth mechanism and the supporting evidence, Nano Lett. 3 (7) (2003) 955–960.
[14] Y. Sun, Y. Yin, B.T. Mayers, T. Herricks, Y. Xia, Uniform silver nanowires synthesis by reducing $AgNO_3$ with ethylene glycol in the presence of seeds and poly(vinyl pyrrolidone), Chem. Mater. 14 (2002) 4736–4745.
[15] K.K. Caswell, C.M. Bender, C.J. Murphy, Seedless, surfactantless wet chemical synthesis of silver nanowires, Nano Lett. 3 (5) (2003) 667–669.
[16] A.-X. Zhai, X.-H. Cai, X.-Y. Jiang, G.-Z. Fan, A novel and facile wet-chemical method for synthesis of silver microwires, Trans. Nonferrous Metals Soc. China 22 (4) (2012) 943–948.
[17] J.-Q. Hu, Q. Chen, Z.-X. Xie, G.-B. Han, R.-H. Wang, B. Ren, Y. Zhang, Z.-L. Yang, Z.-Q. Tian, A simple and effective route for the synthesis of cristalline silver nanorods and nanowires, Adv. Funct. Mater. 14 (2) (2004) 183–189.
[18] N.R. Jana, L. Gearheart, C.J. Murphy, Wet chemical synthesis of silver nanorods and nanowires of controllable aspect ratio, Chem. Commun. 7 (2001) 617–618.
[19] S.-H. Zhang, Z.-Y. Jiang, Z.-X. Xie, X. Xu, R.-B. Huang, L.-S. Zheng, Growth of silver nanowires from solutions — a cyclic penta-twinned-crystal growth mechanism, J. Phys. Chem. 109 (2005) 9416–9421.
[20] F.K. Liu, P.W. Huang, Y.C. Chang, F.H. Ko, T.C. Chu, Microwave-assisted synthesis of silver nanorods, J. Mater. Res. 19 (2) (2004) 469–473.
[21] A. Schoenhals, F. Kremer, Broadband dielectric spectroscopy, in: F. Kremer, SA (Eds.), Analysis of Dielectric Spectra, Springer, Berlin, 2003, pp. 59–98.
[22] S. Havriliak, S. Negami, A complex plane analysis of a-dispersions in some polymers systems, 14 (1) (1966) 99–117.
[23] P.A.M. Steeman, J. van Turnhout, A numerical Kramers–Kronig transform for the calculation of dielectric relaxation losses free from Ohmic conduction losses, Colloid Polym. Sci. 275 (2) (1997) 106–115.
[24] S. Chisca, V.E. Musteata, I. Sava, M. Bruma, Dielectric behavior of some aromatic polyimide films, Eur. Polym. J. 47 (5) (2011) 1186–1197.

[25] M.-D. Damaceanu, V.-E. Musteata, M. Cristea, M. Bruma, Viscoelastic and dielectric behaviour of thin films made from siloxane-containing poly(oxadiazole-imide)s, Eur. Polym. J. 46 (5) (2010) 1049–1062.
[26] A.C. Comer, D.S. Kalika, B.W. Rowe, B.D. Freeman, D.R. Paul, Dynamic relaxation characteristics of Matrimid® polyimide, Polymer 50 (3) (2009) 891–897.
[27] H. Montès, K. Mazeau, J.Y. Cavaillé, Secondary mechanical relaxations in amorphous cellulose, Macromolecules 30 (1997) 6977–6984.
[28] S. Kirkpatrick, Percolation and conduction, Rev. Mod. Phys. 45 (4) (1973) 574–588.
[29] W. Zheng, X. Lu, W. Wang, Z. Wang, M. Song, Y. Wang, C. Wang, Fabrication of novel Ag nanowires/poly(vinylidene fluoride) nanocomposite film with high dielectric constant, Phys. Status Solidi (a) 207 (8) (2010) 1870–1873.
[30] G.A. Gelves, B. Lin, U. Sundararaj, J.A. Haber, Low electrical percolation threshold of silver and copper nanowires in polystyrene composites, Adv. Funct. Mater. 16 (18) (2006) 2423–2430.
[31] G. Stauffer, Introduction to percolation theory. In: Francis Ta, editor., 1985.
[32] N.F. Mott, E.A. Davis, Electronic Processes in Non Crystalline Materials, Calendron Press, Oxford, 1979.